Ferroelectrics

ISSN: 0015-0193 (Print) 1563-5112 (Online) Journal homepage: https://www.tandfonline.com/loi/gfer20

Ferroelectric Domains in $PbTiO_3/SrTiO_3$ Superlattices

P. Zubko , N. Jecklin , N. Stucki , C. Lichtensteiger , G. Rispens & J.-M. Triscone

To cite this article: P. Zubko , N. Jecklin , N. Stucki , C. Lichtensteiger , G. Rispens & J.-M. Triscone (2012) Ferroelectric Domains in $PbTiO_3/SrTiO_3$ Superlattices, Ferroelectrics, 433:1, 127-137, DOI: 10.1080/00150193.2012.678159

To link to this article: https://doi.org/10.1080/00150193.2012.678159

Ferroelectrics, 433:127–137, 2012

ISSN: 0015-0193 print / 1563-5112 online
DOI: 10.1080/00150193.2012.678159

Taylor & Francis
Taylor & Francis Group

Ferroelectric Domains in $PbTiO_3/SrTiO_3$ Superlattices

P. ZUBKO,[1,*] N. JECKLIN,[1] N. STUCKI,[2]
C. LICHTENSTEIGER,[1] G. RISPENS,[1] AND J.-M. TRISCONE[1]

[1]DPMC, University of Geneva, 24 quai Ernest-Ansermet,
1211 Geneva-4, Switzerland
[2]Hepia, University of Applied Sciences HES-SO, 4 rue de la Prairie,
1202 Genève, Switzerland

Polydomain superlattices composed of ferroelectric $PbTiO_3$ and paraelectric $SrTiO_3$ were investigated by means of temperature-dependent X-ray diffraction and electrical measurements. The ferroelectric nanodomains were found to have an almost isotropic distribution of domain wall alignments and to be highly responsive to applied electric fields, giving rise to large enhancements in the overall dielectric response of the structure. Electrical measurements revealed a dramatic dependence of the dielectric permittivity, tunability, and polarization-voltage characteristics on the superlattice period. For short-period superlattices, double hysteresis loops were observed.

Keywords Ferroelectric nanodomains; Oxide superlattices; Double hysteresis; X-ray diffraction

I. Introduction

Since the seminal work of Esaki and Tsu in 1970 [1], research on semiconducting superlattices—single crystalline semiconductors with a periodic variation of chemical composition—has unveiled new physical phenomena and has led to numerous novel devices, some of which have seen commercial success. Crucial to this success was the development of high quality epitaxial thin film deposition techniques. Over the past two decades, the oxides community has also seen tremendous progress in thin film growth methods, opening the possibility of combining complex oxides and their diverse physical properties into epitaxial heterostructures such as multilayers and superlattices. In many cases, the properties of such heterostructures go well beyond a simple combination of those of the parent compounds, as the effects of strain and dimensionality, as well as competition between different phases, coupling of structural instabilities and symmetry breaking at interfaces yield fascinating and often unpredictable behavior [2]. One class of such heterostructures are superlattices composed of ferroelectric and paraelectric perovskites [3–6].

As we celebrate the 70th birthday of Prof. James F. Scott, whose name has become synonymous with ferroelectric memories, we also celebrate the many advances in our understanding of ferroelectric thin films and devices [47, 48]. With the continuing need for device miniaturization and the promise of new nanoscale components, such as ferroelectric

Received January 19, 2012.
*Corresponding author. E-mail: pavlo.zubko@unige.ch

tunnel junctions, much of the focus has shifted towards ultrathin ferroelectrics. Here, ferroelectric/paraelectric superlattices offer an excellent alternative to metal-ferroelectric-metal capacitors for studying ferroelectricity in the ultrathin limit. Moreover, numerous studies have shown that these artificial crystals offer a powerful method for tailoring their ferroelectric properties by simply altering the thicknesses of the individual layers [7–11], and at the same time exhibit interesting interface phenomena [12]. Strain and electrostatics are the main parameters governing the response of these materials, and both can be used to dramatically modify their behavior. Using X-Ray diffraction and second harmonic generation, Scott's group was the first to expose the full complexity of the structure of $BaTiO_3/SrTiO_3$ super lattices arising from the competition between the strain and electrostatic energies [6, 51].

The importance of ferroelectric domains in superlattices has been addressed in a number of experimental [10, 13–16] and theoretical studies [17–21], with unusual domain morphologies and dynamics predicted by ab initio based methods [22]. It is only recently, however, that such domains have been directly observed experimentally in superlattices composed of $PbTiO_3$ (PTO) and $SrTiO_3$ (STO) [15], $BiFeO_3$ and $SrTiO_3$ [50], and, most recently, in the $BaTiO_3/SrTiO_3$ system [23]. In the former, ordered arrays of ferroelectric nanodomains give rise to in-plane satellites in the X-ray diffraction (XRD) reciprocal space maps (RSM), analogous to those found in pure ultrathin films of PTO [24–26], and were linked to large enhancements in the dielectric response [15]. In this article, the structural and electrical characterization of such polydomain PTO/STO superlattices is presented.

II. Experimental

PTO/STO superlattices were grown by off-axis radio frequency magnetron sputtering on commercial (001) $SrTiO_3$ monocrystalline substrates, polished and etched by the manufacturer (Crystek) to obtain TiO_2 terminated surfaces. PTO was deposited from a 10% Pb-excess target ($Pb_{1.1}TiO_3$) to compensate for Pb volatility; a stoichiometric target was used for STO. Both materials were deposited at a substrate temperature of 530°C (monitored by a thermocouple inside a resistive heater) in an O_2/Ar mixture of ratio 24:29 with a total pressure of 0.18 Torr. Epitaxial top and bottom $SrRuO_3$ (SRO) electrodes were deposited at 640°C in 0.1 Torr O_2/Ar atmosphere of ratio 1:20.

Structural analysis was performed with a PANalytical X'Pert PRO diffractometer using CuKα_1 radiation. An Anton Paar DHS 900 hotstage was used for high temperature measurements. Specular scans were obtained with a triple axis detector, whereas a PIXcel line detector was used to record the RSMs. X-ray diffraction measurements were used to determine the average out-of-plane lattice parameters and superlattice periodicities. In-plane coherence with the substrate was confirmed by looking at RSMs around the $(\bar{1}03)$ Bragg peaks of the substrate and by comparing the rocking curves of the substrate and the film. Atomic force microscopy revealed smooth surfaces with a mean roughness of a few Å and one unit cell high steps due to the miscut of the underlying substrate. For samples with SRO electrodes, two-unit-cell-high steps were sometimes observed.

Ferroelectric hysteresis loops were measured with an AixACCT 2000TF ferroelectric tester using a triangular waveform of 100 Hz or 1 kHz. Dielectric data were obtained with an Agilent 4284A precision LCR meter using a 1 kHz, 10–100 mV signal.

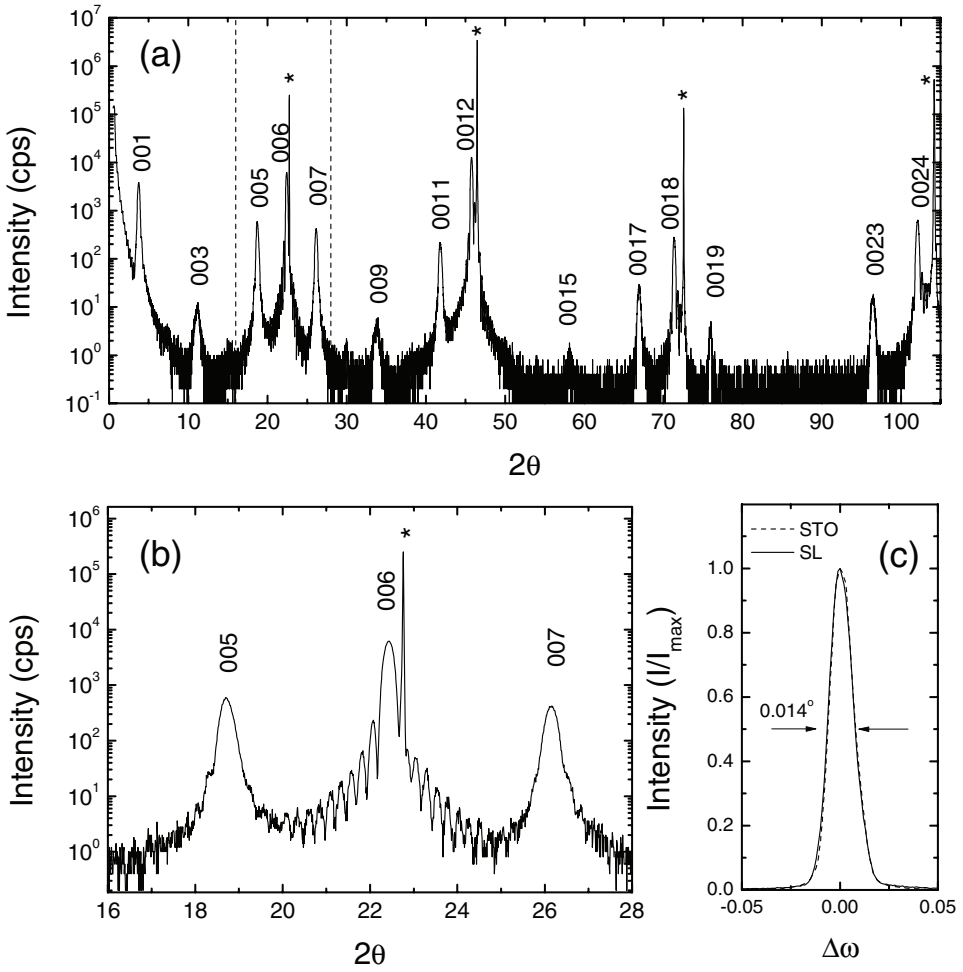

Figure 1. (a) Specular crystal truncation rod for a $(3|3)_{15}$ superlattice showing the $(00l)$ superlattice peaks corresponding to the artificially imposed periodicity of 6 perovskite u.c. Reflections due to the underlying STO substrate are marked with a star. The region between the dashed lines has been expanded horizontally in (b) to show the Laue oscillations between the superlattice peaks due to the finite overall thickness of the structure. (c) Normalized rocking curves for the substrate and superlattice Bragg peaks.

III. X-Ray Diffraction Measurements

A. Superlattice Structure

A representative specular crystal truncation rod is shown in Fig. 1(a). For an $(n_p|n_s)_m$ superlattice with n_p unit cells of PTO and n_s unit cells of STO repeated m times, the positions of the superlattice reflections depend only on the average out-of-plane lattice parameter $\bar{c} = (n_p c_p + n_s c_s)/(n_p + n_s)$ and the number of unit cells in the repeating unit $N = (n_p + n_s)$, appearing at $Q_z = \frac{2\pi l}{\bar{c}N}$ with $l = 0,1,2\ldots$. The individual lattice parameters c_p and c_s of PTO and STO affect only the intensities of the reflections and cannot be obtained from the peak positions. Sharp superlattice reflections as well as Laue oscillations due to the

finite thickness of the overall structure are clearly visible in Fig. 1(b), indicating well defined superlattice periodicities and layer thicknesses. RSMs reveal identical in-plane lattice parameters for the superlattice and the substrate. The very small in-plane lattice mismatch between bulk tetragonal PTO and STO, however, makes it difficult to assess the coherency of the structure from RSMs as, even in the presence of dislocations, the relaxed in-plane lattice parameters of the superlattice and the underlying substrate will be very similar. For this reason, rocking curves (ω-scans) were also compared. As shown in Fig. 1(c), when normalized by their maximum intensities, the rocking curves for the substrates and super-lattices are identical, confirming the fully epitaxial growth. The excellent crystalline quality of the superlattices was further confirmed by scanning transmission electron microscopy [27].

B. Domain Structure

Diffuse X-ray scattering has been used extensively to investigate in-plane ordering and defect structure of different compounds. In this way, nanoscale periodic ferroelectric 180° domains have recently been observed in $PbTiO_3$ ultrathin films [24–26, 28]. Figure 2 shows reciprocal space maps around several superlattice reflections. Each reflection is

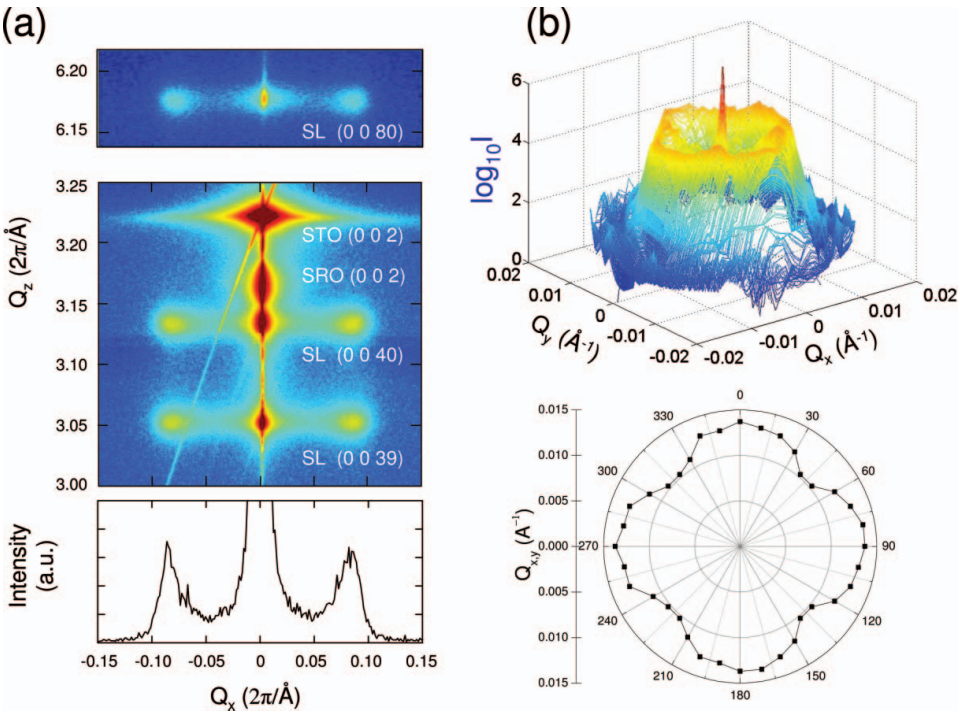

Figure 2. (a) Reciprocal space maps around the specular crystal truncation rod of a $(13|7)_{13}$ superlattice with SRO electrodes showing diffuse satellites that accompany the superlattice (SL) Bragg reflections. The line profile is taken across a set of satellites along an in-plane (Q_x) direction in reciprocal space. (b) The domain satellites in this $(13|3)_{12}$ superlattice form a distorted ring around the SL Bragg peak in Q_x–Q_y space indicating a slight in-plane anisotropy of the domain periods, with domain sizes being smaller when the domain walls are parallel to the ⟨100⟩ crystallographic axes. The bottom graph is a polar plot of the satellite peak positions.

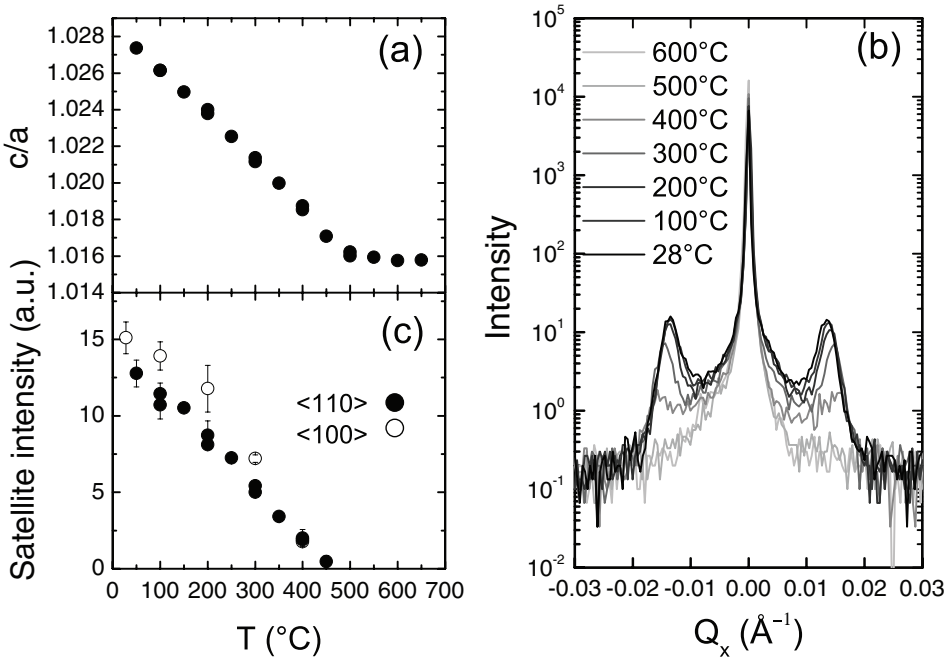

Figure 3. Temperature dependence of (a) tetragonality, (b) domain satellites along ⟨100⟩ and (c) their intensities along ⟨100⟩ and ⟨110⟩, showing the disappearance of domain satellites in the paraelectric phase.

accompanied by distinct satellite peaks, corresponding to an in-plane periodicity of around 75 Å. Associating these peaks with a regular array of 180° ferroelectric domains requires some care, as similar satellites can arise for a number of other reasons. Ordered arrays of dislocations [29, 30] and point defects, ferroelastic domains [31] and other periodic structural modulations [32, 33] are known to produce similar peaks. Substrate miscut effects can also generate apparent in-plane periodicity due to the intersection of the film Bragg peaks with the crystal truncation rod [34]. Studies of $PbTiO_3$ thin films have been careful to rule out these effects [25, 26]. Figure 3 shows the temperature evolution of the lattice parameters and the satellite peak intensities for a $(13|17)_{62}$ superlattice. The sample tetragonality $\bar{c}/a$ decreases linearly on approaching the ferroelectric-to-paraelectric transition temperature T_c, plateauing in the paraelectric phase. Concomitantly, the intensity of the satellite peaks progressively decreases with temperature until they finally disappear in the paraelectric phase. Subsequent cooling leads to reappearance of the domain satellites, with the same periodicity, in the ferroelectric phase. This confirms that the satellite peaks are related to the ferroelectric domain structure. The large overall thickness of the superlattices also allows uniform electric fields to be applied and the response of the domains to be imaged simultaneously using XRD. Changes in domain satellite peak intensities (but not positions) were observed under applied field, indicating that the relative sizes of the "up" and "down" domains are modified as the material is polarized, whereas the overall domain period remains constant [15].

To rule out the possibility of regular ferroelastic *ac* domains, which are known to form in $PbTiO_3$ films on $DyScO_3$ substrates [31], we note the following three things: (i) unlike

for $DyScO_3$ substrates, the in-plane lattice parameter of $SrTiO_3$ is almost identical to that of tetragonal PTO and hence the formation of *a* domains, which would normally accommodate the tensile strain in the film, is not expected. (ii) Our films remain tetragonal in the high-temperature paraelectric phase and hence if ferroelastic domains were present, there would be no reason to expect them to disappear at T_c. (iii) Ferroelastic domains generally form very regular patterns, with domain walls aligned along specific crystallographic directions [31, 35]. As shown in Fig. 2, the regular domain structures of our films are observed for any in-plane direction, reminiscent of what is seen in pure PTO thin films [24, 36]. Regarding the domain periodicity, in some cases no detectable anisotropy is observed, while in others the domain periods along the ⟨100⟩ crystallographic directions are smaller than those along ⟨100⟩, suggesting that domain walls that are not aligned with the crystallographic axes are energetically more costly. For ultrashort-period superlattices, the reverse is found.

C. Electrostatic Coupling

A detailed discussion of the electrostatic interactions between the ferroelectric layers can be found in Ref. 37. Here, only the main results are summarized.

The domain sizes were found to increase with the thickness of the individual PTO layers following the same trend as domains in ultrathin PTO films studied by Streiffer *et al*. [24]. This suggests that the ferroelectric layers are not strongly interacting, with the exception of very fine period superlattices (with $n_S \lesssim 3$ u.c.) which have larger domain sizes due to the stronger electrostatic coupling between the PTO layers [37]. Domains in PTO thin films investigated by Streiffer and co-workers [24, 25] were found to evolve as a function of temperature. The polydomain state just below T_c was termed the α-phase. Upon cooling, the domain sizes increased, saturating at a value approximately $\sqrt{2}$ times larger (β-phase). One proposed explanation for the two different phases was a change in screening as ionic adsorbates accumulate on the top surface at lower temperatures, reducing the depolarizing field in the system [24, 25, 38]. At room temperature, the PTO films were found to be in the monodomain state. Interestingly, the domain sizes in PTO/STO superlattices are in excellent quantitative agreement with those of the β-phase, despite the fact that all interfaces in the system are identical and no significant screening by free charges is expected. This finding may lend support to other proposed explanations for the different polydomains states in PTO thin films, such as changes in domain morphology and domain wall energy [25, 26].

The evolution of the lattice parameters with temperature for a selection of superlattices with $n_P = n_S$ is shown in Figs. 4(a) and b. The sample tetragonality in this case decreases in a non-linear way on approaching the phase transition temperature. The transition temperatures of the superlattices increase with PTO layer thickness, matching those of PTO thin films of the corresponding thickness, consistent with the idea that the PTO layers are not strongly interacting. Only for superlattices with $n_S \lesssim 3$ u.c. was a deviation from this behavior observed, indicating stronger electrostatic coupling between the ferroelectric layers. The crossover from coupled to decoupled behavior in PTO/STO superlattices thus happens at much lower paraelectric layer thicknesses than in the analogous $KNbO_3/KTaO_3$ system investigated by Specht *et al.* [13]. This is surprising given that the dielectric constant of STO is higher than that of $KTaO_3$, and may be related to either differences in the dielectric permittivities of the ferroelectric layers or the extent of cation interdiffusion across the interfaces. For PTO/STO superlattices, electron energy loss spectroscopy measurements have confirmed that any intermixing or surface roughness is confined to within ± 1 u.c. of the interface. Diffusion over larger length scales would effectively increase the thickness of the ferroelectric layers resulting in a stronger coupling between them.

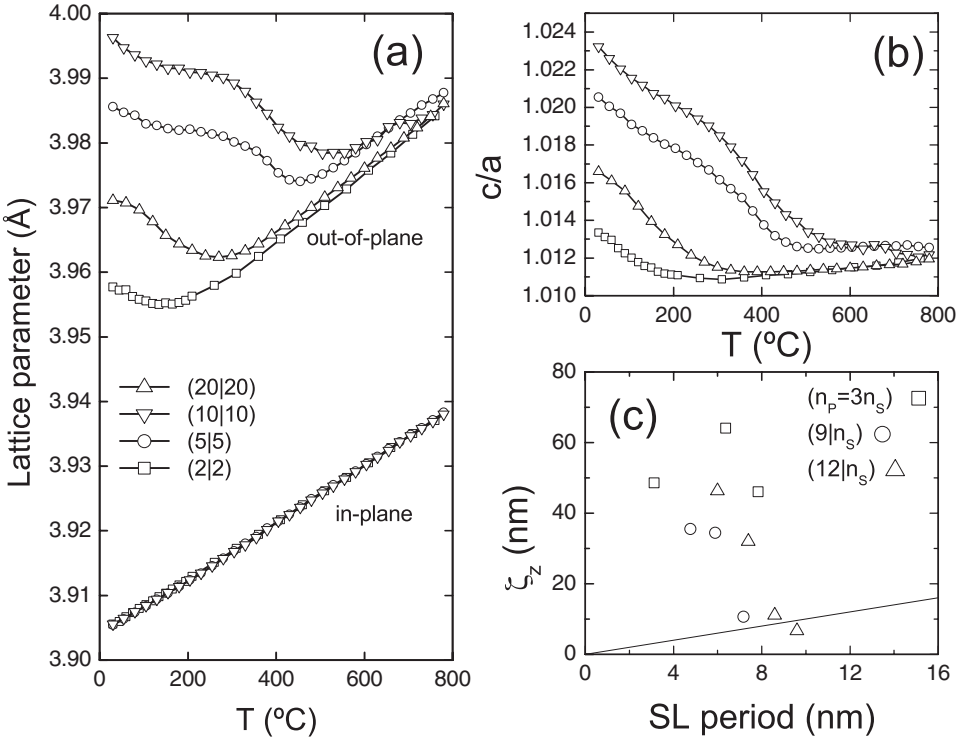

Figure 4. Temperature dependence of (a) the out-of-plane $\bar{c}$ and in-plane a lattice parameters, and (b) the tetragonality $(\bar{c}/a)$ used to determine the transition temperatures. (c) Out-of-plane coherence lengths ζ_z along Q_z of the domain satellites for three series of superlattices: with a fixed PTO volume fraction of 0.75 (i.e. $n_p = 3n_s$, □), and with fixed PTO layer thicknesses of 9 u.c. (◯) and 12 u.c. (△). The solid line $\zeta_z = N\bar{c}$ separates regions with coherence lengths larger and smaller than the superlattice period $N\bar{c}$.

Analysis of the full widths at half maxima (FWHM) of the domain satellite peaks along the Q_z reciprocal space direction provides information about the out-of-plane coherence length ζ_z, which can be determined using the Scherrer equation. Although measurements of domain sizes and transition temperatures give no obvious indication of significant electrostatic interactions between the ferroelectric layers for $n_S \gtrsim 3$ u.c., the large out-of-plane coherence lengths ζ_z indicate that domain structures are nevertheless well aligned over many superlattice periods (Fig. 4(c)). As expected, ζ_z decreases with increasing STO layer thickness, approaching length scales comparable to the individual PTO layer thicknesses. Note, all ζ_z values provide lower limits on the true coherence length as other sources of peak broadening may contribute to the reduction of ζ_z. For superlattices with larger periodicities, ζ_z could not be determined accurately due to the close proximity of the superlattice Bragg peaks that leads to merging of adjacent domain satellites.

IV. Electrical Properties

One advantage of studying nanodomains in superlattices is the dramatic reduction in leakage currents as compared to ultrathin ferroelectric films [11], opening the possibility of applying

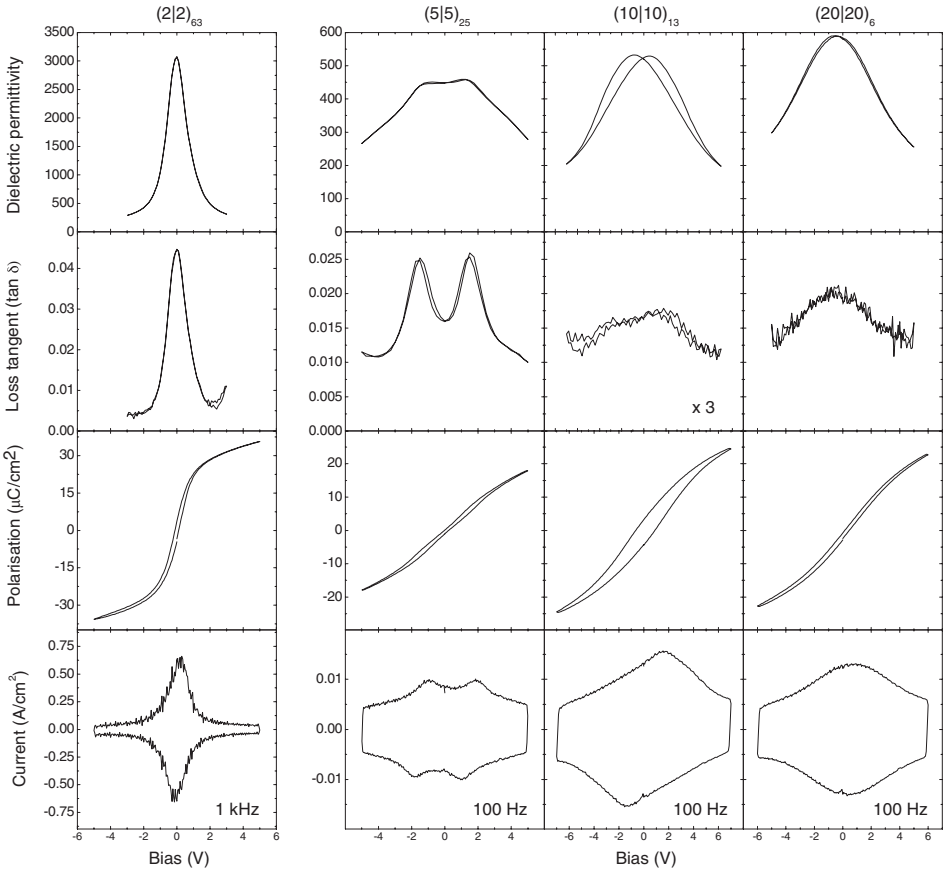

Figure 5. Evolution of electrical properties (dielectric permittivity, loss tangent, polarization-voltage loops and the corresponding switching currents) with superlattice periodicity for ($n|n$) heterostructures. The dielectric permittivities and loss tangents were measured with a 1 kHz, 100 mV ac bias (50 mV for the $(10|10)_{13}$ sample).

large uniform electric fields in conventional parallel plate capacitor geometry [15]. The larger thickness of the superlattices also reduces the effects of the dielectric/electrode interfaces, which are usually detrimental to the ferroelectric properties. Figure 5 shows the evolution of the field-dependent dielectric response and the polarization-voltage loops with superlattice periodicity. When the individual layers are just one or two unit cells thick, a very large and highly tunable dielectric response is observed. The large value of the permittivity can in part be attributed to the close proximity to the ferroelectric-to-paraelectric phase transition with $T_c \approx 400$ K as determined from XRD measurements of the lattice parameters. Dielectric measurements revealed a relatively broad dielectric anomaly, typical of thin films and very similar to that observed in (Pb,Sr)TiO_3 films [39]. In the (1|1) and (2|2) superlattices, every PTO layer is in contact with at least one STO layer, hence the effects of intermixing must also be considered and may explain the similarity to the solid solution behavior. Interface effects discussed in Refs.12 and 40 are also expected to strongly influence the properties of these ultra-fine-period superlattices.

A dramatic change in behavior is observed upon increasing the superlattice periodicity to (3|3) or higher, i.e. once there is at least one full PTO and STO monolayer per period that experiences a bulk-like chemical environment. The permittivity drops significantly and the capacitance-voltage curves develop a minimum at zero bias. Superlattices with 4, 5 and 6 u.c. thick layers, corresponding to samples with the smallest domain sizes, behave in a qualitatively similar way, as illustrated by the $(5|5)_{25}$ sample in Fig. 5. As the bias increases, the capacitance curves exhibit maxima, and very weak hysteresis is observed upon cycling. This behavior is accompanied by the appearance of double hysteresis in the polarization-voltage loops and is reminiscent of the response of a typical antiferroelectric. In an antiferroelectric material two interpenetrating sublattices with opposite polarization form the ground state of the system and the independent switching of these sublattices leads to the double hysteresis. In our case, the very fine 180° domain structure is in some ways similar to the antiparallel dipole arrangement of an antiferroelectric, albeit on the scale of several unit cells (rather than a single unit cell).

Capacitance-voltage curves similar to that of the $(5|5)_{25}$ sample in Fig. 5 have been reported previously in $KNbO_3/KTaO_3$ (1|1) superlattices. Electric fields were applied in-plane using interdigitated electrodes [41], and the authors concluded that the individual layers were coupled antiferroelectrically. Later it was shown that fine period $BaZrO_3/SrTiO_3$ superlattices also exhibit a similar response, while increasing the individual layer thicknesses led to appearance of ferroelectricity [42]. Unlike these previous reports, here the antiferroelectric-like response is observed for out-of-plane fields, suggesting that it may be related to the ferroelectric nanodomain structure rather than a true antiferroelectric coupling between the dipoles of neighboring unit cells.

At this point, it should be noted that double hysteresis loops can arise in ferroelectric materials for a number of reasons other than antiferroelectricity. In $BaTiO_3$ single crystals, just above T_c, a ferroelectric state can be induced by application of an electric field, giving rise to double hysteresis [43]. In $BiFeO_3$, double hysteresis loops were interpreted in terms of a field-induced structural phase transition from a paraelectric orthorhombic to a ferroelectric rhombohedral state [44]. Pinched hysteresis loops are also a common feature of aged, hard (acceptor-doped) $Pb(Zr,Ti)O_3$ (PZT) ceramics. The acceptor dopants are compensated by the formation of oxygen vacancies, which are mobile at temperatures when the PZT undergoes its ferroelectric-to-paraelectric phase transition. If the samples are cooled slowly through the transition, the defect dipoles align themselves parallel to the polarization within each domain, pinning the polydomain state [45]. At lower temperatures, these defect dipoles provide a restoring force that hinders polarization reversal and results in double hysteresis loops. Repeated cycling at high fields and elevated temperatures can disorder the defect dipoles, restoring switchable polarization and opening the polarization hysteresis loop [46].

Although defect dipole-induced domain pinning cannot be ruled out conclusively in our case, unlike for hard PZT [46] repeated switching of the superlattices at 10 Hz and at 400 kV/cm for 10000 cycles did not lead to any opening of the hysteresis loop, even at elevated temperatures of up to 130°C. We therefore believe that at room temperature, the restoring force for the stripe domain state comes from the depolarizing fields that arise in the PTO layers for any non-zero macroscopic polarization. These depolarizing fields are a consequence of the partial decoupling of the PTO layers, as discussed in section III C. At low temperatures, however, domain wall pinning by defects is important and leads to domain wall freezing with a corresponding dramatic reduction in permittivity.

Upon cooling to low temperatures, the double-hysteresis loops gradually open up and evolve into conventional ferroelectric loops. A detailed discussion of the low temperature

properties of superlattices in the weakly coupled regime will be published elsewhere. For still higher superlattice periods, slim ferroelectric hysteresis loops and weakly hysteretic capacitance-voltage curves are observed (Fig. 5). The narrow hysteresis and the large dielectric constants (as compared to the expected intrinsic lattice response for these compositions) can be attributed to domain wall motion, as was explicitly shown to be the case in a previous study [15]. Unlike in typical bulk ferroelectrics or in thicker films, where ferroelectric switching proceeds through inhomogeneous nucleation and growth of ferroelectric domains [47, 48], in the case of superlattices no nucleation is required as the polydomain state is inherent to these heterostructures. Moreover, due to the very small domain sizes (of the order of a few nanometers), tiny domain wall displacements can give rise to very large and reversible changes in the macroscopic polarization [15]. However, although domain walls never need to move more than a few lattice spacings to fully saturate the polarization, complete switching is hindered by the development of a large depolarization field in the heterostructure [49].

V. Conclusions

In summary, the domain structure and dielectric and ferroelectric properties of PTO/STO superlattices were studied using a combination of XRD and electrical measurements. The ferroelectric nanodomains form regular periodic structures that give rise to in-plane satellites around the superlattice Bragg reflection with a quasi-isotropic distribution of domain wall orientations. Electrostatic interactions between the ferroelectric layers are strongly reduced for STO layer thicknesses larger than ~ 3 u.c. Nevertheless, the domain structures remain coherent over many superlattice periods with a coherence length that progressively decreases with increasing STO layer thickness. As the superlattice period is varied, a dramatic evolution of the electrical properties is observed. Superlattices with ultrashort periods display a very large and highly tunable dielectric response, whereas for superlattices with 3–6 u.c. thick layers of PTO and STO double hysteresis is observed. Further measurements are necessary to elucidate the precise physical origin of this behavior.

Acknowledgments

The authors thank Prof. Jim Scott for many fascinating and inspiring discussions. P.Z. is also grateful to Prof. Igor Luk'yanchuk for illuminating discussions during a visit to Amiens. Marco Lopes is gratefully acknowledged for technical support. This work was funded by the Swiss National Science Foundation through the National Center of Competence in Research, Materials with Novel Electronic Properties (MaNEP) and Division II; the EU project OxIDes; and the Leverhulme Trust.

References

1. L. Esaki and R. Tsu, *IBM Journal of Research and Development* **14**, 61 (1970).
2. P. Zubko, S. Gariglio, M. Gabay, P. Ghosez, and J.-M. Triscone, *Annual Review of Condensed Matter Physics* **2**, 141 (2011).
3. H. Tabata, H. Tanaka, and T. Kawai, *Applied Physics Letters* **65**, 1970 (1994).
4. D. O'Neill, R. M. Bowman, and J. M. Gregg, *Applied Physics Letters* **77**, 1520 (2000).
5. T. Shimuta *et al.*, *Journal of Applied Physics* **91**, 2290 (2002).
6. A. Jiang, J. Scott, H. Lu, and Z. Chen, *J. Appl. Phys.* **93**, 1180 (2003).
7. J. B. Neaton and K. M. Rabe, *Appl. Phys. Lett.* **82**, 1586 (2003).
8. K. Johnston, X. Huang, J. B. Neaton, and K. M. Rabe, *Phys. Rev. B* **71**, 100103 (2005).

9. H. N. Lee, H. M. Christen, M. F. Chisholm, C. Rouleau, and D. H. Lowndes, *Nature* **433**, 395 (2005).
10. D. A. Tenne *et al.*, *Science* **313**, 1614 (2006).
11. M. Dawber *et al.*, *Advanced Materials* **19**, 4153 (2007).
12. E. Bousquet *et al.*, *Nature* **452**, 732 (2008).
13. E. D. Specht, H.-M. Christen, D. P. Norton, and L. A. Boatner, *Phys. Rev. Lett.* **80**, 4317 (1998).
14. M. P. Warusawithana, E. V. Colla, J. N. Eckstein, and M. B. Weissman, *Phys. Rev. Lett.* **90**, 036802 (2003).
15. P. Zubko, N. Stucki, C. Lichtensteiger, and J.-M. Triscone, *Phys. Rev. Lett.* **104**, 187601 (2010).
16. J. Y. Jo *et al.*, *Phys. Rev. Lett.* **107**, 055501 (2011).
17. M. Sepliarsky, S. R. Phillpot, D. Wolf, M. G. Stachiotti, and R. L. Migoni, *Phys. Rev. B* **64**, 060101 (2001).
18. V. A. Stephanovich, I. A. Luk'yanchuk, and M. G. Karkut, *Phys. Rev. Lett.* **94**, 047601 (2005).
19. Y. L. Li *et al.*, *Appl. Phys. Lett.* **91**, 252904 (2007).
20. S. Lisenkov and L. Bellaiche, *Phys. Rev. B* **76**, 020102 (2007).
21. A. P. Levanyuk and I. B. Misirlioglu, *Journal of Applied Physics* **110**, 114109 (2011).
22. S. Lisenkov, I. Ponomareva, and L. Bellaiche, *Phys. Rev. B* **79**, 024101 (2009).
23. K. Kathan-Galipeau *et al.*, *ACS Nano* **5**, 640 (2011).
24. S. K. Streiffer *et al.*, *Phys. Rev. Lett.* **89**, 067601 (2002).
25. D. D. Fong *et al.*, *Science* **304**, 1650 (2004).
26. R. Takahashi, O. Dahl, E. Eberg, J. K. Grepstad, and T. Tybell, *Journal of Applied Physics* **104**, 064109 (2008).
27. A. Torres-Pardo *et al.*, *Phys. Rev. B* **84**, 220102(R) (2011).
28. G. Catalan *et al.*, *Phys. Rev. Lett.* **96**, 127602 (2006).
29. V. M. Kaganer, R. Köhler, M. Schmidbauer, R. Opitz, and B. Jenichen, *Phys. Rev. B* **55**, 1793 (1997).
30. V. M. Kaganer, O. Brandt, A. Trampert, and K. H. Ploog, *Phys. Rev. B* **72**, 045423 (2005).
31. A. H. G. Vlooswijk *et al.*, *Applied Physics Letters* **91**, 112901 (2007).
32. S. J. May *et al.*, *Nature Materials* **8**, 892 (2009).
33. A. Vailionis *et al.*, *Applied Physics Letters* **95**, 152508 (2009).
34. C. Aruta *et al.*, *Phys. Rev. B* **65**, 195408 (2002).
35. G. Catalan *et al.*, *Nature Materials* **10**, 963967 (2011).
36. C. Thompson *et al.*, *Applied Physics Letters* **93**, 182901 (2008).
37. P. Zubko *et al.*, *Nano Letters* **12**, 2846 (2012).
38. S. Prosandeev and L. Bellaiche, *Phys. Rev. B* **75**, 172109 (2007).
39. M. Jain *et al.*, *Appl. Phys. Lett.* **91**, 072908 (2007).
40. P. Aguado-Puente, P. Garcia-Fernandez, and J. Junquera, *Phys. Rev. Lett.* **107**, 217601 (2011).
41. J. Sigman, D. P. Norton, H. M. Christen, P. H. Fleming, and L. A. Boatner, *Phys. Rev. Lett.* **88**, 097601 (2002).
42. H. M. Christen, E. D. Specht, S. S. Silliman, and K. S. Harshavardhan, *Phys. Rev. B* **68**, 020101 (2003).
43. W. J. Merz, *Phys. Rev.* **91**, 513 (1953).
44. D. Kan *et al.*, *Advanced Functional Materials* **20**, 1108 (2010).
45. K. Carl and K. H. Haerdtl, *Ferroelectrics* **17**, 473 (1978).
46. M. I. Morozov and D. Damjanovic, *Journal of Applied Physics* **104**, 034107 (2008).
47. J. F. Scott, *Ferroelectric Memories* (Springer-Verlag, Berlin, Germany, 2000).
48. M. Dawber, K. M. Rabe, and J. F. Scott, *Rev. Mod. Phys.* **77**, 1083 (2005).
49. V. Nagarajan *et al.*, *Journal of Applied Physics* **100**, 051609 (2006).
50. R. Ranjith U. Lüders, W. Prellier, A. DaCosta, I. Dupont, and R. Desfeux. *Journal of Magnetism and Magnetic Materials*, **321**, 1710 (2009).
51. Rios *et al.*, *J. Phys. Condens. Matter.* **15**, L305 (2003).